JGR Space Physics

RESEARCH ARTICLE
10.1029/2021JA029242

Advection of Martian Crustal Magnetic Fields by Ionospheric Plasma Flow Observed by the MAVEN Spacecraft

I. de Oliveira[1,2], M. Fränz[2], E. Echer[1], and A. Franco[1]

[1]National Institute for Space Research, São José dos Campos, Brazil, [2]Max-Planck-Institute for Solar System Research, Göttingen, Germany

Key Points:

- The crustal magnetic fields on Mars are being displaced relative to their expected location
- The displacement increases with solar zenith angle and altitude
- Ionospheric plasma flow is most likely responsible for this process

Supporting Information:

Supporting Information may be found in the online version of this article.

Correspondence to:

I. de Oliveira,
oliveira@mps.mpg.de

Citation:

de Oliveira, I., Fränz, M., Echer, E., & Franco, A. (2021). Advection of Martian crustal magnetic fields by ionospheric plasma flow observed by the MAVEN spacecraft. *Journal of Geophysical Research: Space Physics*, *126*, e2021JA029242. https://doi.org/10.1029/2021JA029242

Received 15 FEB 2021
Accepted 23 AUG 2021

Abstract The plasma environment of Mars is highly influenced by its crustal magnetic fields. In this work, we investigate whether the crustal magnetic fields can be displaced from their original positions due to advection by ionospheric plasma flow. The ranges of interest are altitudes between 200 and 1,000 km and solar zenith angles between 45° and 135°. We examine magnetic field data using measurements from the Magnetometer (MAG) onboard the Mars Atmosphere and Volatile EvolutioN (MAVEN) spacecraft. We conduct statistical analyses (~5 years of data) in order to investigate if horizontal shifts are observed between the data and the crustal magnetic field model by Langlais et al. (2019), https://doi.org/10.1029/2018je005854. We also show two case studies of individual measurements within a specific region of Mars. The results show statistical and observational evidence that the crustal magnetic fields are often being advected towards the night-side of the planet. The displacement seems to increase exponentially as a function of altitude, reaching a horizontal shift of 100 km at 650 km altitude. Moreover, we use measurements from the SupraThermal And Thermal Ion Composition (STATIC) instrument in order to compare the dynamic pressure of ionospheric plasma flow to the magnetic pressure of the crustal magnetic fields. There are two possible causes for the displacement: a forcing by external magnetic pressure or an advection of the field to the electron fluid, which follows the ion fluid. In this paper, we argue that by the observed relation between ion fluid and displacement, the latter explanation is more probable.

Plain Language Summary Crustal magnetic fields keep information of a past time, when Mars still had its own internal magnetic field generator. These structures do not tend to change in the long-term, so several models have been built throughout the last decades with the aim of reproducing the observed Martian fields. The crustal fields can influence the dynamics of the atmosphere. The region of the atmosphere, which is dominated by atmospheric plasma (ions and electrons) is the ionosphere. At Mars, the ionosphere lies at ~130 km and above. In theory, the flow of the plasma is able to move the crustal magnetic fields in a process called advection. In this work, we indicate that this process happens often at Mars. Our results may be important for improving crustal magnetic field models, and also for estimating how much electricity the ionospheric plasma can conduct.

1. Introduction

Although Mars does not presently possess an intrinsic dynamo-generated magnetic field, remanent magnetic features are common in the planet's crust. Localized crustal magnetic sources on Mars were first discovered by the Mars Global Surveyor spacecraft, in September 1997 (Acuña et al., 1998). These small-scale magnetic fields are mostly associated with the heavily cratered and ancient terrain of the Southern hemisphere and they indicate that magnetic activities had occurred in the planet's interior in the past (Acuña et al., 2001; Connerney et al., 1999, 2004).

Several works have shown that crustal magnetic fields can prevent regions of the Martian atmosphere from interacting directly with the solar wind (Brain, 2006; Mitchell et al., 2001). This provokes significant changes in ionospheric parameters, such as composition (Withers et al., 2015), density (Gurnett et al., 2008), ion flows (Fan et al., 2020), and escape fluxes (Fang et al., 2017), as well as changes in the heights of plasma boundaries (Brain et al., 2005; Crider, 2004; Mitchell et al., 2001).

At the same time, the interaction with the electromagnetic fields caused by the solar wind flow at high altitudes can lead to an expansion of crustal field loops in the anti-solar direction and cause the formation of magnetic flux ropes in the ionosphere (Brain et al., 2010; Hara et al., 2015, 2017; Vignes et al., 2004). The magnetic flux ropes eventually detach and the ionospheric plasma contained inside them escapes from the planet's atmosphere.

Here, we decide to investigate the opposite, namely whether the ionospheric flow can influence the crustal magnetic fields on Mars at altitudes where the solar wind has no direct influence. In this paper, we specifically investigate whether an observed displacement of the magnetic fields is consistent with the direction of the horizontal plasma flow, at low altitudes (~200–1000 km).

There are some similarities between this process and the formation of magnetic flux ropes by the solar wind. However, at lower altitudes, the most likely physical cause is advection by ionospheric flow, while at higher altitudes, it is best explained by an interaction with flowing solar wind plasma.

This paper is divided into seven sections. The next section is a summary of the theory behind our idea. In Sections 3 and 4, the data and the methods used in this work are described. In Section 5, the results are presented. Two case studies are shown in Section 6. The conclusions are given in Section 7.

2. The Advection of the Magnetic Fields

In an ionized environment, a plasma velocity field can provoke changes in a magnetic field. This process is clearly expressed in terms of the induction equation, given as

$$\frac{\partial \boldsymbol{B}}{\partial t} = \nabla \times (\boldsymbol{u} \times \boldsymbol{B}) + \frac{1}{\mu_0 \sigma} \nabla^2 \boldsymbol{B}, \tag{1}$$

where $\boldsymbol{B}$ is the magnetic field, $\boldsymbol{u}$ is the plasma velocity, μ_0 is the permeability of free space, and σ is the parallel electrical conductivity of the plasma. The induction equation states that the rate at which the magnetic field changes in time depends on its advection by the plasma velocity (first term on the right-side) and its diffusion through the plasma (second term on the right-side).

Advection is a physical process in which a quantity is transported by a velocity field, in the same direction of the field. If the plasma has a very high conductivity ($\sigma \to \infty$), the magnetic field lines are carried along with the flux, in the so called "frozen-in" condition, first introduced by Alfvén (1942). Conversely, if the plasma is a poor conductor, the magnetic fields contained within it will diffuse over time. For a general discussion of the advection of magnetic fields, see Davidson (2001), Lui (2018), and Wilmot-Smith et al. (2005).

Mars' ionosphere is composed of a plasma with finite conductivity, which means that the magnetic fields are affected by both advection and diffusion. The parallel conductivity reaches 1000 S/m at ~200 km, and increases very slowly with altitude, as can be seen in Figure 26.6a from Fillingim (2018).

As a first approximation, ionospheric plasma flow is supposed to be mostly horizontal and directed towards the night-side of the planet because of the day-to-night pressure gradient. Besides that, we also assume that the parallel conductivity is roughly constant in the selected range of altitudes. In a stagnant situation where this condition happens, the magnetic field would always diffuse back to its original position if there is an increase of dynamic or thermal pressure from the topside.

In the case of the Earth's magnetosphere, the plasma below the magnetopause has a very low resistivity, such that pressure pulses acting on the magnetopause lead to a compression of the internal field on very short time scales (Fowler, 2005). At Mars and Venus, pressure pulses are damped by the highly resistive ionospheric plasma and an internal field can react on external pressure changes only on time scales of 30 min to hours (Luhmann & Cravens, 1991). On the other hand, the thermal pressure in the ionosphere increases with decreasing solar zenith angle, which leads to ion acceleration towards the night side. The electron fluid partly connected to the ions and partly to the crustal fields must react to this acceleration.

A possible effect of the externally induced magnetic fields can also not be excluded, but the external field at Mars usually leads to magnetization of the lower ionosphere, causing an internal magnetic pressure which decreases with altitude (Ma et al., 2019). In principle, gradients in this magnetization could also cause a displacement of the crustal fields, so this possibility is not ruled out.

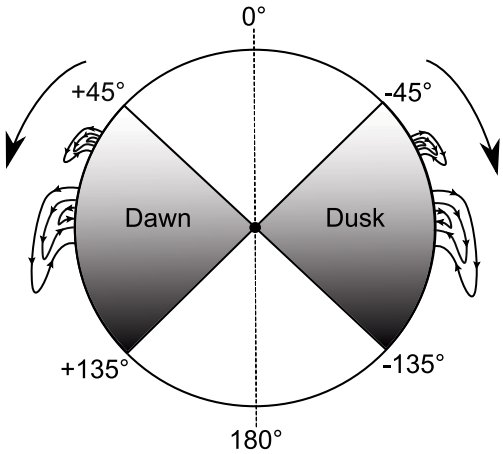

Figure 1. Illustration of the advection of magnetic fields on Mars, viewed from the perspective of the North Pole (big dot in the center). The large arrows indicate the general day-to-night direction of ionospheric plasma flow. The numbers refer to the solar zenith angles (SZA). The gray regions represent the SZA ranges used for defining the dawn-side and dusk-side data sets.

3. Data

The analyzed data are obtained by the NASA's spacecraft Mars Atmosphere and Volatile EvolutioN (MAVEN), detailed by Jakosky et al. (2015). The data are selected for altitudes between 200–1000 km.

For the magnetic field, we use data provided by the Magnetometer (MAG) instrument (Connerney et al., 2015), reformatted into common data file format (CDF) and resampled at 4 s cadence, from October 2014 to February 2020. We also use ion spectra for O^+ and O_2^+ ions observed from October 2014 to November 2018 by the SupraThermal And Thermal Ion Composition (STATIC) instrument (McFadden et al., 2015).

The time ranges of the two data sets differ because not all of the ion data have been processed yet, by the time of writing. However, it is important to clarify that for the pressure analysis (Section 4.2) and the case studies (Section 6), we use the same time range for both data sets (until November 2018) for consistency.

The STATIC instrument operates in different modes providing different data products with different mass, energy, angular, and time resolution. For our studies, we use the method described in Dubinin et al. (2017) and interpolate the STATIC products C6, C8, CA, D1, CF, and CD to obtain a joint product with 32 energy steps, 4 inclination angles, 16 azimuth angles, 8 ion masses, and 4 s time resolution. The joint product is normalized such that the energy flux integrated along each dimension agrees with the integral of each of the source products. From this joint product, we determine the plasma moments density, velocity, and thermal pressure for the ion species H^+, O^+, and O_2^+ corrected for spacecraft velocity and potential according to Fränz et al. (2006) and Lavraud and Larson (2016).

In addition to the data, the crustal magnetic field model built by Langlais et al. (2019) is also used in our analyses. This model combines magnetic field data from NASA's Mars Global Surveyor and MAVEN to derive a high-resolution model of Mars' crustal magnetic field, based on equivalent source dipoles and spherical harmonic functions. We should note that this model is obtained by long time averages of both day-side and night-side observations, where effects of external magnetic fields have been largely filtered out.

Figure 1 illustrates the process of advection of the magnetic fields, which are dragged away in the day-to-night direction, as well as the ranges of solar zenith angles (SZA) used in this work.

The data are selected for SZA between ±45° and ±135°. Here, we add a sign to the zenith angle, where positive values of SZA mark the "dawn-side" data set and negative values mark the "dusk-side" data set. The data with SZA between +45° and 45° are excluded due to the strong induced magnetic field and turbulent ionospheric behavior that exists in that region. The night-side data with SZA between +135° and 135° are also not considered because of the weak ionospheric flow, which is unlikely to displace the crustal magnetic fields.

We focus our data analysis on the radial component of the magnetic field (B_r). The piled-up magnetic field on Mars, which originates in the compressed interplanetary magnetic field (IMF) on the day-side of the planet, is mostly horizontal and reaches intensities only up to a few nT in its radial component (Brain et al., 2003; Withers, 2009). Therefore, B_r is the component least affected by the day-side induced field (Arkani-Hamed, 2004). Besides that, the cross-product $\boldsymbol{u} \times \boldsymbol{B}$ (Equation 1) is maximum for B_r, under the assumption of a horizontal plasma velocity $\boldsymbol{u}$.

In Section 6, we use solar wind data for a brief discussion of upstream conditions. These data are measured at the spacecraft position with the largest magnetopause normal distance from October 2014 to November 2018 (1 measurement per orbit). Velocity and density data are provided by the Solar Wind Ion Analyzer instrument (Halekas et al., 2015), and IMF components are taken from the MAG instrument.

4. Statistical Analyses

We perform two statistical analyses of long-term data to directly detect the effects of the crustal magnetic field advection and to compute the relative forces between the moving ionospheric plasma and the magnetic field structures. The methodology and the results of the two types of analyses are presented in the following subsections.

4.1. Shifting Technique

To search for evidence of advection on Mars means to search for a spatial shift of the crustal magnetic fields along the mean plasma flow lines. In a first approximation, these flow lines are along the day-to-night parallels with constant clock angle. We develop a simple method based on the direct comparison between two magnetic field maps, after one of the maps has been shifted, or displaced, longitudinally.

If we assume that the shift is towards the night-side and neglect the inclination of Mars, the shift vector would be $(s \times \cos(L), s \times \sin(L))$, where s is total shift in degrees and L is the latitude measured from the equator.

If we calculate the mean shift in the latitude range 0°–75° and take only the longitudinal shift, we make an error in each bin of $\varepsilon = s \times \sin(L)$. The mean error is then

$$\varepsilon_{mean} = \frac{\int_0^{75} s \times \sin(L)\, dL}{\int_0^{75} s\, dL} = 56\% \tag{2}$$

This would mean that we underestimate the true shift by 56%. If we would, for example, only consider the range 0°–30°, the error would become only 25%.

In any case, we are always underestimating the true shift by this method. As we know, the best method would have been to bin the data and the model values in a clock angle × SZA coordinate system, but this is less intuitive than working in longitude × latitude grids.

Another way of justifying the choice of shifting the maps only in the east-west direction is because the possible causes of advection do not have strong polar components. If the fields are displaced by ionospheric plasma flow, this would be more easily observed in the east-west direction, because the azimuthal component is the major contributor to the horizontal plasma velocity (see Figure S1).

If however, the fields are displaced due to the interaction with the solar wind, this would also be observed in the east-west direction, because the solar wind travels in the Sun-Mars direction across the ecliptic. Since we expect the total displacement of the magnetic fields to be small, a shift in the north-south direction would be very hard to spot statistically.

Radial magnetic field maps of the data and of the computed model are produced for eight altitude ranges, every 100 km between 200–1000 km. We use a regular grid, with bin sizes of 0.5° for both longitude and latitude. The choice of small bin sizes is justified as we expect the displacement to be small.

As a consequence of the small bin size, there is a median of 2 data points per bin only. That means that the effects of the changing external field and pressure may not cancel out for a single bin, but they will when the statistical average over the complete map is taken.

MAVEN spacecraft has not yet covered all bins of that map, which means there are gaps in the data. For a total of 216,000 bins per map, the number of bins with data points decreases with altitude, varying from ~110000 at lower altitudes to ~60000 at higher altitudes (Figure S2).

For each altitude range, the observations are subtracted from the magnetic field model, at every respective bin, and the total sum of the residuals ($\Delta B'$ [nT]) is calculated as

$$\Delta B' = \frac{1}{j} \sum_{i=1}^{j} |B_{r\,i}^{M} - B_{r\,i}^{O}|, \tag{3}$$

where j is the number of bins that belong to both maps, and B_r^M and B_r^O are the radial components of the model and of the observed magnetic field, respectively. $\Delta B'$ is a qualitative index only. Bins with no data points are not taken into consideration for this calculation.

While the maps of MAVEN observations are kept in a fixed position, the maps of the magnetic field model are shifted longitudinally between 5.0° (westwards) and +5.0° (eastwards), with steps of 0.5°. For each step, a new $\Delta B'$ is calculated. This simple procedure is done for dawn-side and dusk-side data sets individually. In total, we have 16 small data sets.

We assume that the minimum value of $\Delta B'$ corresponds to a position where the magnetic field model matches the observations the most. If the advection of the crustal magnetic fields occurs often, we expect to see the minimum value of $\Delta B'$ at some offset different from zero, for each set of results. Besides that, we also expect the offset to be directed towards the night-side, i.e., westwards at the dawn-side and eastwards at the dusk-side (see Figure 1).

For each data set, the results of $\Delta B'$ can be fitted to an inverted Gaussian function. We calculate the offsets by taking the minimum $\Delta B'$ of each fitted curve. At this point, we have one value of offset for each of the 16 data sets. We apply an exponential regression to the offsets.

In order to simplify the interpretation of the results, the longitudinal shifts (LS) in degrees are converted into equivalent equatorial distances (EED) in km, as a function of altitude, according to the expression:

$$EED = \frac{2\pi\ LS}{360}(r + altitude), \tag{4}$$

where $r = 3393.5$ km is the mean Mars' radius.

4.2. Pressure Analysis

To investigate the force balance between ionospheric plasma flow and the crustal magnetic fields, we compare the pressures related to the advection process. On the one hand, the dynamic pressure of the ionospheric flow "pushes" towards the night-side. On the other hand, the crustal magnetic structures compensate with their magnetic pressure. If the dynamic pressure overcomes the magnetic pressure, the ionospheric flow is more likely to move the magnetic field structures, dragging them with it.

For the calculation of the dynamic pressure [Pa], we use ionospheric data of low energy O^+ and O_2^+ ions obtained by STATIC, which are the major contributors for Mars' ionosphere composition (Benna et al., 2015; Carlsson et al., 2006). Its equation is given as

$$p_{dyn} = \frac{\rho u^2}{2}, \tag{5}$$

where ρ [kg/m^3] is the mass density of the particles and u [m/s] is their horizontal flow speed. u is calculated as the vector addition of the median azimuthal velocity and the median polar velocity for each bin.

The magnetic pressure [Pa] is computed from the data as

$$p_{mag} = \frac{B^2}{2\mu_0}, \tag{6}$$

where B [T] is the total intensity of the magnetic field and $\mu_0 \simeq 4\pi \times 10^{-7}$ H/m.

The data are analyzed in terms of SZA × altitude, and classified according to the intensity of the crustal magnetic field model calculated at an altitude of 400 km. Regions where $B \leq 10$ nT are defined as weak magnetic fields (~68% of the total area) and regions where $B > 10$ nT are defined as strong magnetic fields (~32% of the total area).

We use bin sizes of 40 km in altitude and 5° in SZA. The median numbers of data points per bin are 842 and 522 at regions of weak and strong magnetic fields, respectively, which is in accordance to the relative sizes of the two areas.

The ratio between the dynamic and the magnetic pressures is calculated and plotted, so we can compare their relative dimensions. These results are presented in the next section. The pressure plots can be seen in Figure S3.

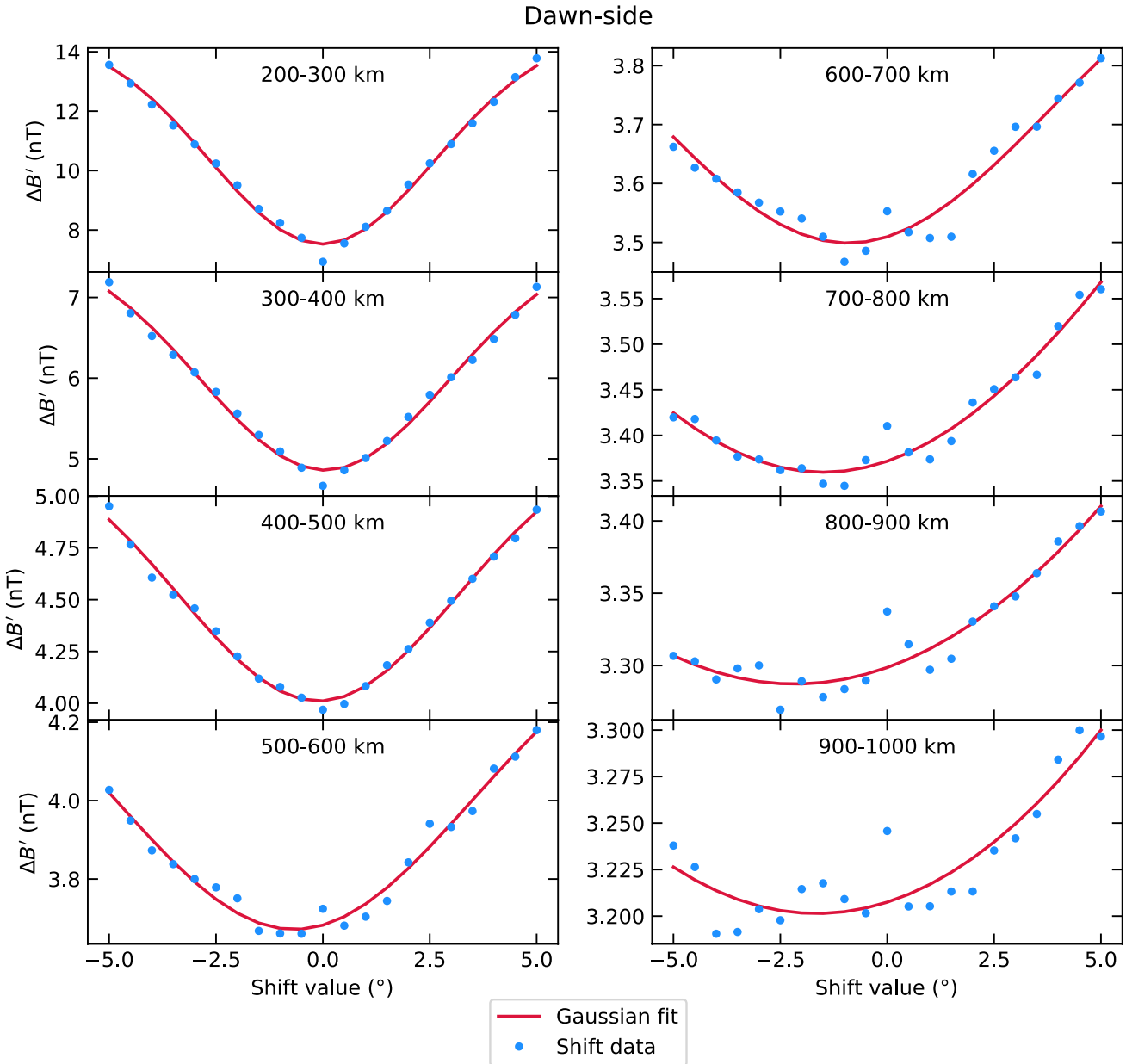

Figure 2. Values of $\Delta B'$ (blue points) for the given longitudinal shift (x-axis) at dawn-side, for each altitude range (stated in the top center of each plot). The red curves are the fitted Gaussian functions. The minimum point of each curve gives the corresponding shift value, or offset, for the respective data set.

5. Results and Discussion

Next, we present the results from the shifting technique (Section 4.1), followed by the results from the pressure analysis (Section 4.2).

Figures 2 and 3 show the values of $\Delta B'$ (blue dots) and the fitted Gaussian (red curve) for each of the 16 data sets, after they were shifted longitudinally every 0.5°. For both dawn- and dusk-side, we observe a larger scatter of $\Delta B'$ for higher altitude ranges, most likely caused by the larger gaps in the data, i.e., less bins with data points. Still, all sets of results present the same behavior and can be fitted by a Gaussian curve, where the minimum value of $\Delta B'$ points to a spatial offset different from zero.

Figure 4 shows the best fit offset values converted to EED as a function of altitude, where each offset value is assumed to be in the center of its corresponding altitude range, e.g., at 250 km for the offsets at 200–300

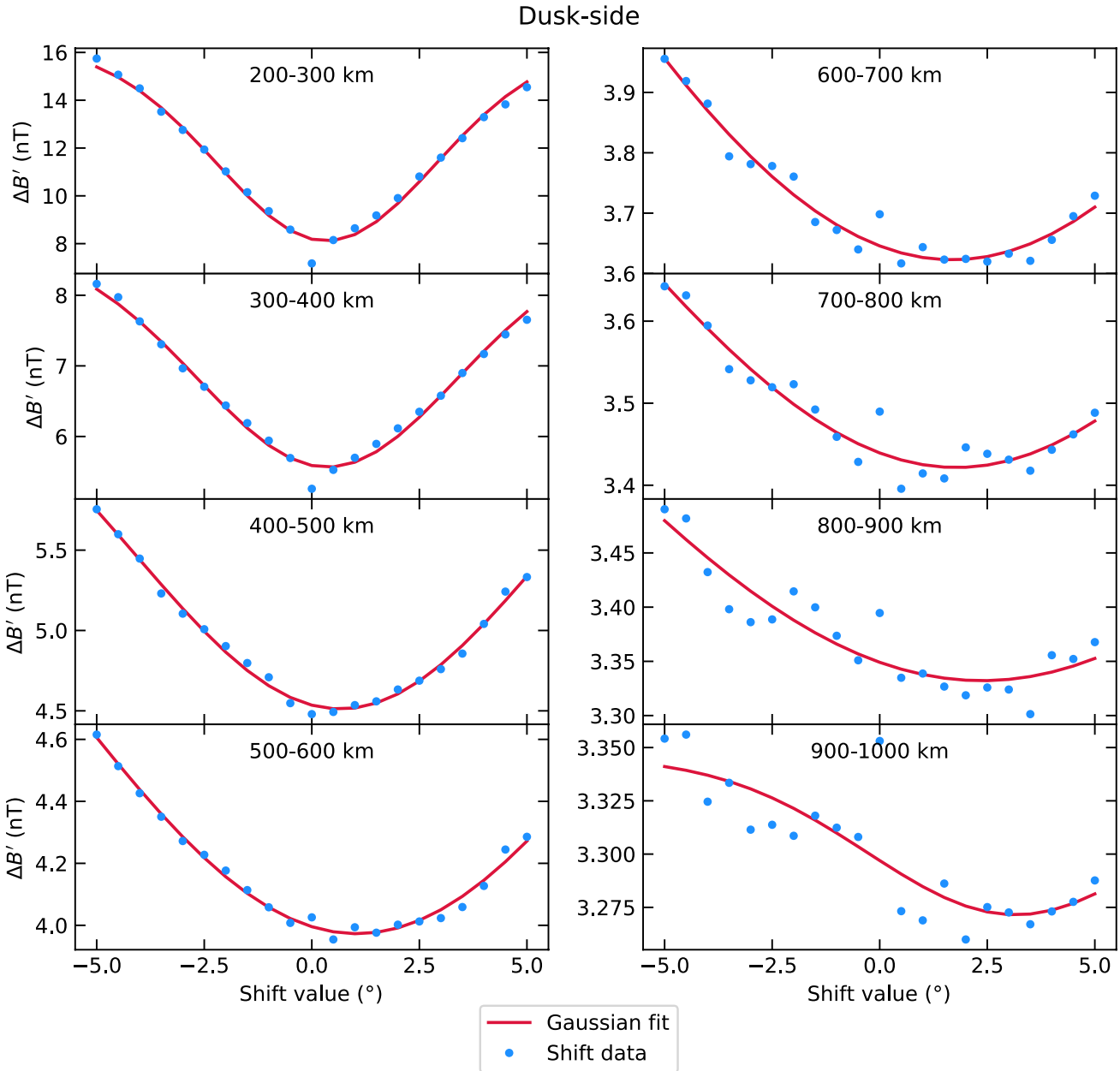

Figure 3. The same as in Figure 2, but for the dusk-side.

km. The bars are the standard deviations of the fits. The red and blue dashed curves are exponential regressions of the dawn- and dusk-side offsets, and the green dashed curve shows the difference between absolute values of the curves.

Statistically, the results of offset at dawn-side are only significant (larger than two standard deviations) from 400 km and upwards, whereas the results at dusk-side are significant for all analyzed altitudes. Therefore, the results infer that the magnetic fields on Mars are indeed being advected.

A few remarks can be made from the results in Figure 4:

1. The absolute offsets generally increase with altitude, indicating that the crustal magnetic fields are being displaced increasingly;
2. The offset directions are towards the night-side of the planet;

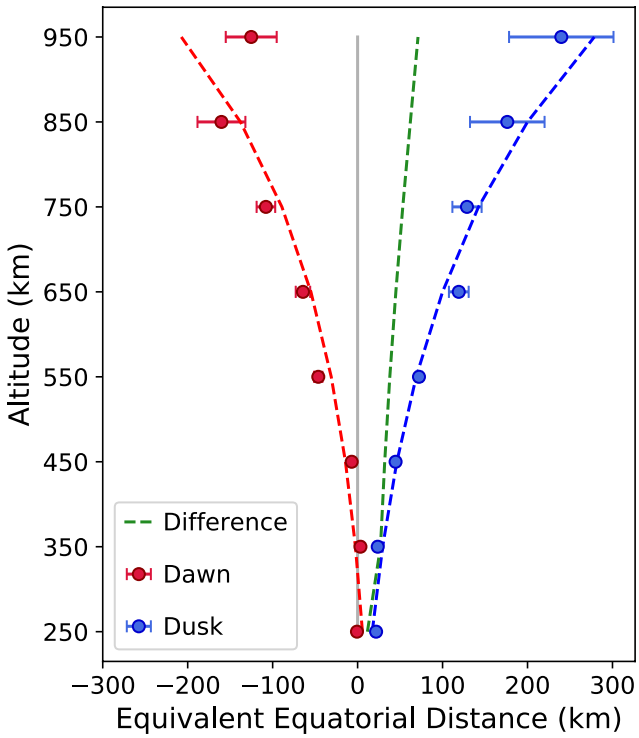

Figure 4. Exponential regression of the longitudinal offsets for minimum $\Delta B'$ at dawn-side (red) and at dusk-side (blue) with their respective standard deviations. The difference between the absolute values of the dusk-side and the dawn-side curves is represented by the green dashed curve. The gray line serves as a reference for the zero offset. The axes are equally scaled.

3. The displacement is larger at the dusk-side than at the dawn-side, which can be seen by the green dashed curve

For the purpose of comparison, the mean horizontal velocity of the ionospheric plasma is calculated at each altitude range in a longitude × latitude grid with bin size of 4°. The results are shown in Figure 5 (see Figure S1 for a glance on the different components).

The horizontal velocities increase towards the night-side as a function of altitude, with dusk-side values increasing at a higher rate. The similarities between figures suggest that the horizontal velocity of the ionospheric flow might be correlated to the advection of the magnetic fields.

Based on the results and on the comparison between Figures 4 and 5, we statistically infer that the magnetic fields are being advected in the same direction of the day-to-night ionospheric flow, and that the magnitude of the displacement is a function of altitude. Although the advection rate is low when we take into account the spatial dimensions of the problem, this displacement might be relevant to detailed studies of Mars' crustal magnetic fields.

Several studies have confirmed the existence of dawn/dusk asymmetries on Mars' ionosphere, e.g., asymmetries related to ion escape fluxes (Kallio et al., 2006), ion densities (Benna et al., 2015), and electron densities (Withers, 2009). We believe that these dawn/dusk asymmetries are also depicted in the advection of the magnetic fields, but this requires further investigation.

Here, we assume that the ionosphere and the crustal magnetic fields are in corotation with the planet. Since the corotation acts against the ion flow on the dawn-side, we could expect a slightly larger advection on the dusk-side. This, and the fact that the horizontal velocities are larger at dusk, may be the reasons why we observe dawn/dusk asymmetries in our results, and more analyses should be done in order to fully understand the asymmetries.

Based on the offsets shown in Figure 4, we give a rough estimate of the advection speed. Consider the altitude range of 600700 km, on the dusk-side of the planet, and a displacement of the crustal field structures of ~120 km. If ionospheric plasma flow has about 6 h to act on the magnetic fields (from SZA = 0° to SZA = 90°), we derive an average advection speed of ~6 m/s. This speed is much slower than the average horizontal plasma speed of 1065 m/s and the corotation speed of 294 m/s, for the same altitude range on the dusk-side.

Next, we present the results obtained by the pressure analysis. Figure 6 shows the ratio between dynamic and magnetic pressures as a function of SZA and altitude for regions of weak (top panels) and strong (bottom panels) magnetic fields. Yellow represents the regions where the dynamic pressure dominates over the magnetic pressure (ratio >1).

From the results shown in Figure 6, we see that the pressure ratio is <1 for almost all selected altitudes and SZA ranges at regions of strong magnetic fields, which means that the dynamic pressure is generally smaller than the magnetic pressure at those regions. Conversely, at regions of weak magnetic background, the ratio is >1 for most of the SZA and altitude ranges, meaning that the dynamic pressure dominates over the magnetic pressure. Also, we see that the dominance of the dynamic pressure at higher altitudes seems to occur at larger SZAs.

In short, the results of the pressure analysis show that ionospheric plasma flow is more likely to cause the advection of the crustal magnetic fields if they are located in a region where the magnetic field background is weak. This is likely to be observed in the Northern hemisphere of the planet, for example.

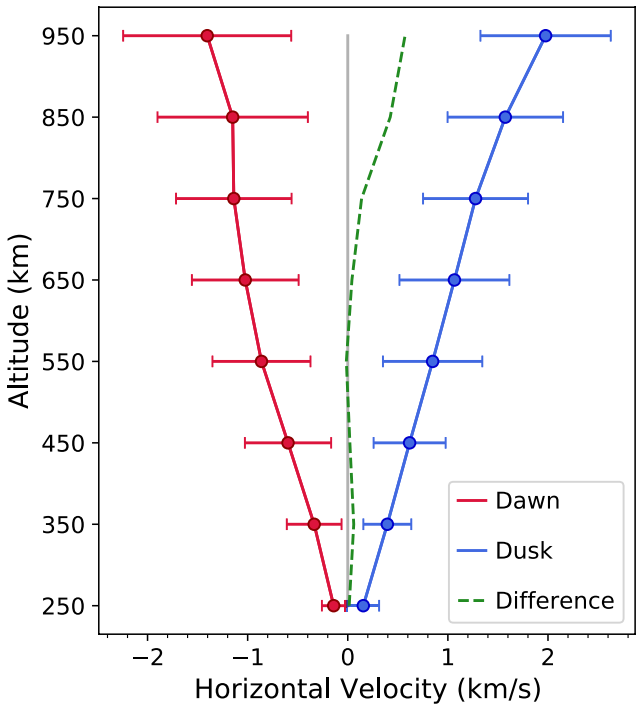

Figure 5. Mean horizontal velocity data of the ionospheric plasma at dawn-side (red) and at dusk-side (blue), and the difference between the absolute dusk- and dawn-side velocities (green). The bars show the standard deviation. The gray line serves as a reference for the null velocity.

It is important to note that the pressure analysis is proposed as a qualitative study with the aim of generally identifying where the advection of the crustal magnetic fields is more likely to occur. In that sense, it is not accurate to claim that the advection occurs exclusively in regions of weak magnetic field.

6. Case Study

We expect to be able to observe the advection of the magnetic fields on local scales. Therefore, a small region of Mars is chosen for a case study. Based on the results of Section 4.2 (Figure 6), we select a region of dipole-shaped magnetic field with weak/moderate intensities in the Northern hemisphere, far from strong sources of magnetization. The region is located between 70°–90° E and 25°–45° N.

We browse through 57 sets of individual measurements of B_r in the selected region (orbital passes). Of these 57 passes, 33 occur in the dawn-side and 24 in the dusk-side. From the 33 orbital passes observed in the dawn-side, 17 show a clear displacement of the magnetic field position when compared to the crustal magnetic field model at the same altitude. Analogously, from the 24 dusk-side passes, 10 show displacement of the field.

The 27 data sets that show displacement are fitted to a nearby position where the total sum of the differences between the observations and the model magnetic field ($\Delta B'$) is minimum, like in the analysis described in Section 4.1 (see Equation 3).

Now, three parameters are varied in order to determine the minimum $\Delta B'$ with better accuracy: longitudinal shift, latitudinal shift, and rotation angle. Assuming that the advection can displace the crustal magnetic fields at different rates for different altitudes, the rotation angle is used for emulating the altitude effect, since the data set is shifted as a whole. We rotate the data counterclockwise (from the North direction) around the point of lowest altitude within the selected region.

We expect the direction of the best fit of each pass to roughly correspond to the average horizontal velocity measured during the pass. From the 27 fits, 16 (59%) are at least in the same direction of the azimuthal component of the ion velocity, and 9 (30%) lie within the same quadrant (i.e., NW, NE, SW, or SE) of the horizontal velocity.

Figures 7 and 8 are two examples of passes in which the fitting direction lies within the same quadrant of the average horizontal direction of the ionospheric flow. The first data set is from 7 May 2016, between ~1804–1809 UT, at the dawn-side of the planet. The second data set was obtained in 2 April 2017, between ~2220–2226 UT, at the dusk-side. In both cases, the altitude of the spacecraft decreases with longitude. Figure S4 shows the position and the altitudes covered by both passes.

In the figures, the magnetic field maps show the position of each data set (circles), as well as the position where they are expected to be (triangles), according to the fits of the longitudinal and latitudinal shifts, and the rotation angle. The arrows on the bottom right corner of each map indicate the direction of the median horizontal velocity ($\overline{V_h}$) of each data set and the direction of the fit, i.e., the direction in which the data set is shifted from its undisturbed position.

In the dawn-side example (Figure 7), the $\Delta B'$ of the unshifted data is 14.98 nT, while this value is 8.29 nT for the fitted data, which corresponds to a reduction of ~45% in the residuals. The fit results in a displacement of 1.5° E and 3.0° S of the magnetic field, with a rotation of 9° counterclockwise. The mean horizontal speed is of 0.32 ± 0.15 km/s, which is an average value according to Figure 5.

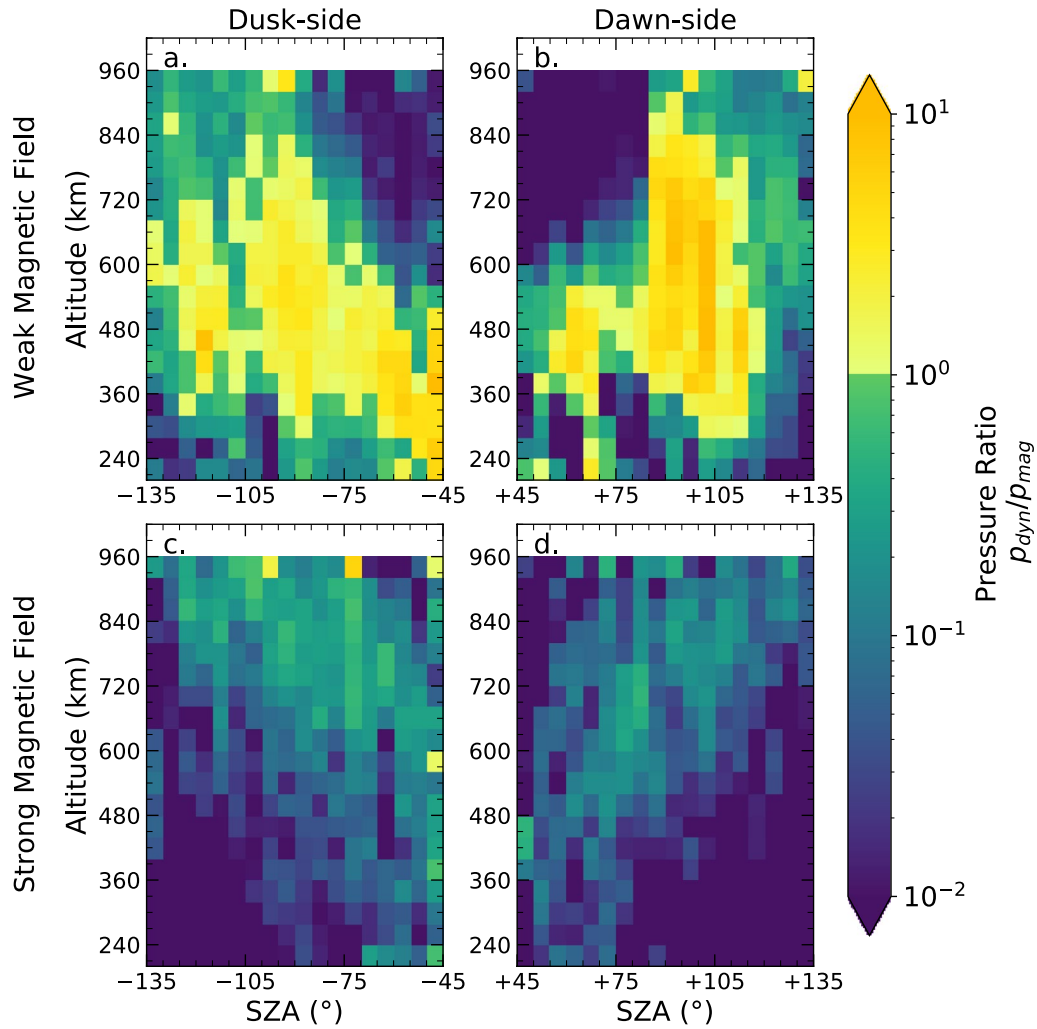

Figure 6. Ratio between dynamic and magnetic pressures as a function of solar zenith angles and altitude. Panels of regions of weak magnetic fields: ratio at (a) dusk-side and at (b) dawn-side. Panels of regions of strong magnetic fields: ratio at (c) dusk-side and at (d) dawn-side. The abrupt change in the color scale defines where the dynamic pressure overtakes the magnetic pressure.

For the dusk-side example (Figure 8), the values of $\Delta B'$ of the unshifted and fitted data are 11.44 and 1.79 nT, respectively. The fit has reduced the residuals by ~85%. The data set is displaced by 3.0° W and 3.5° S, with a rotation angle of 8° counterclockwise. The mean horizontal speed is of 2.23 ± 1.86 km/s, much larger than the average for the corresponding altitude range.

The displacement of the crustal magnetic field seems to be correlated to the speed and direction of ionospheric plasma flow (i.e., larger displacement in the example where the horizontal speed is larger, both towards the day-to-night direction of the ionosphere flow). One could argue that the observed differences are a consequence of the induced magnetic field, once we are looking at individual measurements. However, not only the magnitude of the magnetic field is different from the model, but also the shape of the structure, suggesting a displacement.

To rule out the possibility that the displacements are being caused by upstream conditions of the solar wind, we analyze solar wind data for the 16 orbits where the crustal magnetic field is displaced in the same direction of the azimuthal component of the ion velocity. We compare the dynamic and magnetic pressures of the solar wind during those orbits to the values of those parameters averaged from October 2014 to November 2018. The analysis shows that only one of the passes does not lie within 2 standard deviations

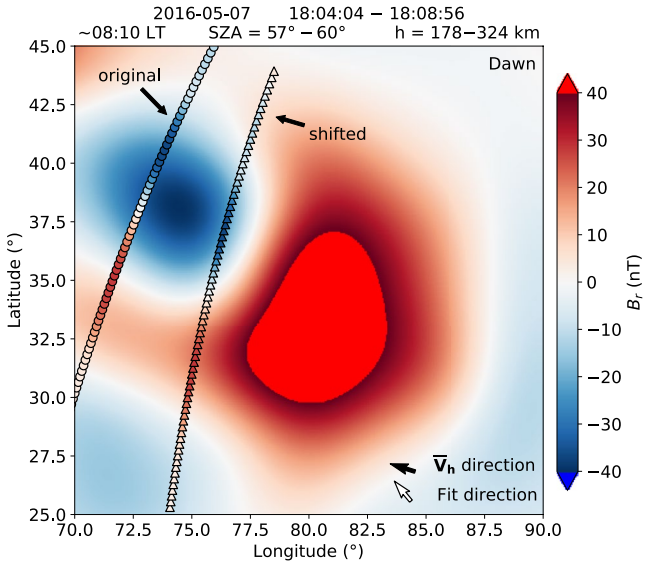

Figure 7. Dawn-side example. The background shows a map of the Langlais et al. (2019) radial crustal magnetic field model at the mean altitude of the measurements. The circles represent the spacecraft trajectory, colored by measured radial magnetic field, while the triangles represent a shift trajectory with the minimum misfit with respect to the crustal field model. The black and the white arrows on the bottom right represent the direction of the median horizontal velocity and the direction of the fit, respectively. The text on the top informs the date, the universal time, the local time, the solar zenith angles range, and the altitude range (h) of the measurements.

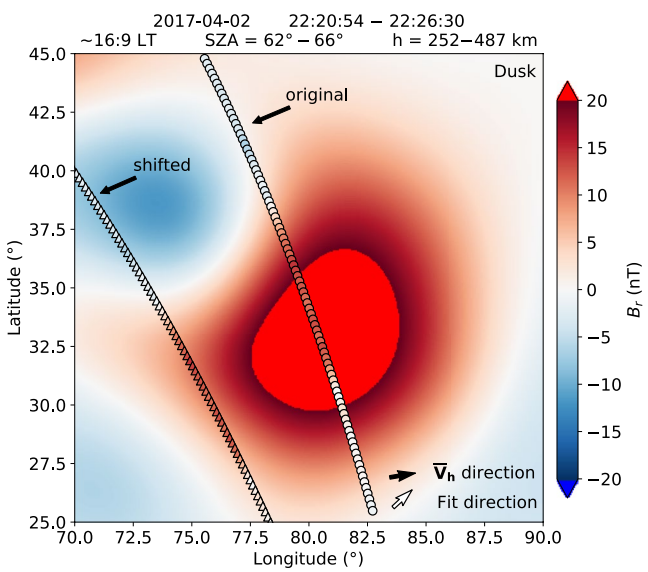

Figure 8. Dusk-side example. Same caption as for Figure 8.

of the dynamic and magnetic pressures, and therefore occur at unusual upstream conditions. Moreover, there are no other large discrepancies during those specific orbits.

From the results shown in the case studies, we infer that the displacement of the magnetic fields in 15 of the 27 observed features is likely to be the caused by the ionospheric flow. This corresponds to 55% of the cases where we see displacement.

7. Conclusions

In this work, we search for advection of the crustal magnetic fields on Mars and investigate the role of ionospheric plasma flow in the process. First, we compare MAVEN magnetic field data from dawn-side and dusk-side to a crustal magnetic field model (Langlais et al., 2019). We compute the residuals on the data, after shifting the model magnetic field longitudinally, and calculate the offsets at which the model fits the data best.

The results from the shifting technique for data at several altitude ranges show the first statistical evidence of advection of the crustal magnetic fields, in which the fields are being displaced towards the night-side of the planet. We evaluate that the fields are being displaced as a function of altitude at a low rate. We roughly derive an advection speed of 6 m/s, at the mean altitude of 650 km, on the dusk-side of the planet.

The advection of the magnetic fields occurs at a higher rate at the dusk-side than at the dawn-side. This implies that this process is influenced by dawn/dusk asymmetries that should be further investigated.

We also analyze the ratio between the dynamic and the magnetic pressures as a function of solar zenith angle and altitude. By comparing these pressures, we show that ionospheric plasma flow could be the responsible for the advection of the crustal magnetic fields at regions of weak magnetic background.

For a case study, we browse through 57 sets of orbital passes on a region of a weak/moderate crustal magnetic fields. We observe displacement of the field in 27 data sets, from which 15 have the offset direction consistent with the azimuthal component of the plasma velocity and occur at periods of average upstream conditions. This leads us to believe that we are observing the advection of the crustal fields due to their interaction with the ionospheric flow.

If we could take the case studies as a global reference, this would mean that we can observe the displacement of crustal fields by ionospheric flow around 26% of the time, at regions of weak/moderate magnetic fields, for SZA near the terminators.

Presently, the calculations used for the case study require significant amount of manual work. Future studies should improve those techniques, as it would help us get a direct measure of velocity versus offset as a function of altitude. Besides that, due to the great variability of altitudes and SZA covered by the MAVEN orbit, the spatial coverage of the spacecraft is still quite sparse. By limiting our longitude × latitude data sets to specific ranges of altitude and SZA and a bin size of 0.5°, we end

up with only a few data points per bin and many gaps in the maps. This means that more detailed analyses, e.g., statistical studies of smaller regions, are not possible yet.

The advection process may be of considerable importance to studies that focus on the variability or on the modeling of the crustal magnetic fields on Mars. The analyses presented in this work might prove to be valuable tools for the estimation of the ionosphere conductivity on Mars. To our knowledge, this is the first observation of magnetic field advection by ionospheric plasma flow in a planetary plasma. Therefore, the ionosphere of Mars is an interesting laboratory to study this plasma physical concept.

Data Availability Statement

All data sets processed for this work are available at https://owncloud.gwdg.de/index.php/s/nQ8iswdeGONNE8Y.

Acknowledgments
We would like to thank the Max-Planck-Institute for Solar System Research for the facilities, data provision, and collaboration. We would like to acknowledge the MAVEN team for gathering and publishing the data at the NASA's Planetary Plasma Interactions Node: https://pds-ppi.igpp.ucla.edu/. Finally, we thank the anonymous reviewers for the great suggestions on how to improve our work. The work was funded by the São Paulo Research Foundation, under grants 2016/10794-2,2017/00516-8, 2018/17098-7, 2018/216557-1, and 2019/01716-6, and by the Brazilian National Council for Scientific and Technological Development, under grants 131260/2018-9, 300234/2019-8, 301883/2019-0, and PQ-302583/2015-7. The data processing at the Max Planck Institute was supported by the German Space Agency under grant 50QM1703. Open access funding enabled and organized by Projekt DEAL.

References

Acuña, M. H., Connerney, J. E. P., Wasilewski, P., Lin, R. P., Anderson, K. A., Carlson, C. W., & Ness, N. F. (1998). Magnetic field and plasma observations at Mars: Initial results of the Mars Global Surveyor mission. *Science*, *279*(5357), 1676–1680. https://doi.org/10.1126/science.279.5357.1676

Acuña, M. H., Connerney, J. E. P., Wasilewski, P., Lin, R. P., Mitchell, D., Anderson, K. A., et al. (2001). Magnetic field of Mars: Summary of results from the aerobraking and mapping orbits. *Journal of Geophysical Research: Plan*, *106*(E10), 23403–23417. https://doi.org/10.1029/2000JE001404

Alfvén, H. (1942). Existence of electromagnetic-hydrodynamic waves. *Nature*, *150*(3805), 405–406. https://doi.org/10.1038/150405d0

Arkani-Hamed, J. (2004). A coherent model of the crustal magnetic field of Mars. *Journal of Geophysical Research: Plan*, *109*(E9), E02008. https://doi.org/10.1029/2004JE002265

Benna, M., Mahaffy, P. R., Grebowsky, J. M., Fox, J. L., Yelle, R. V., & Jakosky, B. M. (2015). First measurements of composition and dynamics of the Martian ionosphere by MAVEN's Neutral Gas and Ion Mass Spectrometer. *Geophysical Research Letters*, *42*(21), 8958–8965. https://doi.org/10.1002/2015GL066146

Brain, D. A. (2006). Mars Global Surveyor measurements of the Martian solar wind interaction. *Space Science Reviews*, *126*(1), 77–112. https://doi.org/10.1007/s11214-006-9122-x

Brain, D. A., Bagenal, F., Acuña, M. H., & Connerney, J. E. P. (2003). Martian magnetic morphology: Contributions from the solar wind and crust. *Journal of Geophysical Research: Space Physics*, *108*(A12). https://doi.org/10.1029/2002JA009482

Brain, D. A., Baker, A. H., Briggs, J., Eastwood, J. P., Halekas, J. S., & Phan, T.-D. (2010). Episodic detachment of Martian crustal magnetic fields leading to bulk atmospheric plasma escape. *Geophysical Research Letters*, *37*(14), L14108. https://doi.org/10.1029/2010GL043916

Brain, D. A., Halekas, J. S., Lillis, R., Mitchell, D. L., Lin, R. P., & Crider, D. H. (2005). Variability of the altitude of the martian sheath. *Geophysical Research Letters*, *32*(18), L18203. https://doi.org/10.1029/2005GL023126

Carlsson, E., Fedorov, A., Barabash, S., Budnik, E., Grigoriev, A., Gunell, H., et al. (2006). Mass composition of the escaping plasma at mars. *Icarus*, *182*(2), 320–328. https://doi.org/10.1016/j.icarus.2005.09.020

Connerney, J. E. P., Acuña, M., Ness, N., Spohn, T., & Schubert, G. (2004). Mars crustal magnetism. *Space Science Reviews*, *111*(1), 1–32. https://doi.org/10.1023/B:SPAC.0000032719.40094.1d

Connerney, J. E. P., Acuña, M. H., Wasilewski, P. J., Ness, N. F., Rème, H., Mazelle, C., & Cloutier, P. A. (1999). Magnetic lineations in the ancient crust of Mars. *Science*, *284*(5415), 794–798. https://doi.org/10.1126/science.284.5415.794

Connerney, J. E. P., Espley, J., Lawton, P., Murphy, S., Odom, J., Oliversen, R., & Sheppard, D. (2015). The MAVEN magnetic field investigation. *Space Science Reviews*, *195*(1), 257–291. https://doi.org/10.1007/s11214-015-0169-4

Crider, D. H. (2004). The influence of crustal magnetism on the solar wind interaction with mars: Recent observations. *Advances in Space Research*, *33*(2), 152–160. https://doi.org/10.1016/j.asr.2003.04.013

Davidson, P. A. (2001). *An introduction to magnetohydrodynamics*: Cambridge University Press. https://doi.org/10.1017/CBO9780511626333.006

Dubinin, E., Fraenz, M., Paetzold, M., McFadden, J., Mahaffy, P. R., Eparvier, F., et al. (2017). Effects of solar irradiance on the upper ionosphere and oxygen ion escape at Mars: MAVEN observations. *Journal of Geophysical Research: Space Physics*, *122*(7), 7142–7152. https://doi.org/10.1002/2017JA024126

Fan, K., Fränz, M., Wei, Y., Cui, J., Rong, Z., Chai, L., & Dubinin, E. (2020). Deflection of global ion flow by the Martian crustal magnetic fields. *The Astrophysical Journal*, *898*(2), L54. https://doi.org/10.3847/2041-8213/aba519

Fang, X., Ma, Y., Masunaga, K., Dong, Y., Brain, D., Halekas, J., et al. (2017). The Mars crustal magnetic field control of plasma boundary locations and atmospheric loss: MHD prediction and comparison with MAVEN. *Journal of Geophysical Research: Space Physics*, *122*(4), 4117–4137. https://doi.org/10.1002/2016JA023509

Fillingim, M. (2018). Ionospheric currents at mars and their electrodynamic effects. In A. Keiling, O. Marghitu, & M. Wheatland (Eds.), *Electric currents in geospace and beyond* (pp. 445–458). American Geophysical Union. https://doi.org/10.1002/9781119324522.ch26

Fowler, G. J. (2005). *The compression of the geo-magnetosphere: A physical model and the effects of compression* (Unpublished doctoral dissertation). University of California, Los Angeles, California, USA.

Fränz, M., Dubinin, E., Roussos, E., Woch, J., Winningham, J. D., Frahm, R., et al. (2006). Plasma moments in the environment of Mars. Mars Express ASPERA-3 observations. *Space Science Reviews*, *126*(1–4), 165–207. https://doi.org/10.1007/s11214-006-9115-9

Gurnett, D. A., Huff, R. L., Morgan, D. D., Persoon, A. M., Averkamp, T. F., Kirchner, D. L., et al. (2008). An overview of radar soundings of the martian ionosphere from the Mars Express spacecraft. *Advances in Space Research*, *41*(9), 1335–1346. https://doi.org/10.1016/j.asr.2007.01.062

Halekas, J. S., Taylor, E. R., Dalton, G., Johnson, G., Curtis, D. W., McFadden, J. P., et al. (2015). The solar wind ion analyzer for MAVEN. *Space Science Reviews*, *195*(1–4), 125–151. https://doi.org/10.1007/s11214-013-0029-z

Hara, T., Brain, D. A., Mitchell, D. L., Luhmann, J. G., Seki, K., Hasegawa, H., et al. (2017). MAVEN observations of a giant ionospheric flux rope near Mars resulting from interaction between the crustal and interplanetary draped magnetic fields. *Journal of Geophysical Research: Space Physics*, *122*(1), 828–842. https://doi.org/10.1002/2016JA023347

Hara, T., Mitchell, D. L., McFadden, J. P., Seki, K., Brain, D. A., Halekas, J. S., et al. (2015). Estimation of the spatial structure of a detached magnetic flux rope at Mars based on simultaneous MAVEN plasma and magnetic field observations. *Geophysical Research Letters*, *42*(21), 8933–8941. https://doi.org/10.1002/2015GL065720

Jakosky, B. M., Lin, R. P., Grebowsky, J. M., Luhmann, D. F., Mitchell, J. G., Beutelschies, G., et al. (2015). The Mars Atmosphere and Volatile Evolution (MAVEN) Mission. *Space Science Reviews*, *195*(1), 3–48. https://doi.org/10.1007/s11214-015-0139-x

Kallio, E., Fedorov, A., Budnik, E., Säles, T., Janhunen, P., Schmidt, W., et al. (2006). Ion escape at mars: Comparison of a 3-D hybrid simulation with mars express IMA/ASPERA-3 measurements. *Icarus*, *182*(2), 350–359. https://doi.org/10.1016/j.icarus.2005.09.018

Langlais, B., Thèbault, E., Houliez, A., Purucker, M., & Lillis, R. (2019). A new model of the crustal magnetic field of Mars using MGS and MAVEN. *Journal of Geophysical Research: Plan*, *124*(6), 1542–1569. https://doi.org/10.1029/2018JE005854

Lavraud, B., & Larson, D. E. (2016). Correcting moments of in situ particle distribution functions for spacecraft electrostatic charging. *Journal of Geophysical Research: Space Physics*, *121*(9), 8462–8474. https://doi.org/10.1002/2016JA022591

Luhmann, J. G., & Cravens, T. E. (1991). Magnetic fields in the ionosphere of Venus. *Space Science Reviews*, *55*(1–4), 201–274. https://doi.org/10.1007/BF00177138

Lui, A. T. Y. (2018). Frozen-in condition for ions and electrons: Implication on magnetic flux transport by dipolarizing flux bundles. *Geoscience Letters*, *5*(5). https://doi.org/10.1186/s40562-018-0104-0

Ma, Y. J., Dong, C. F., Toth, G., van der Holst, B., Nagy, A. F., Russell, C. T., et al. (2019). Importance of Ambipolar electric field in driving ion loss from mars: Results from a Multifluid MHD model with the electron pressure equation included. *Journal of Geophysical Research: Space Physics*, *124*(11), 9040–9057. https://doi.org/10.1029/2019JA027091

McFadden, J. P., Kortmann, O., Curtis, D., Dalton, G., Johnson, G., Abiad, R., et al. (2015). MAVEN SupraThermal and Thermal Ion Composition (STATIC) instrument. *Space Science Reviews*, *195*(1), 199–256. https://doi.org/10.1007/s11214-015-0175-6

Mitchell, D. L., Lin, R. P., Mazelle, C., Rème, H., Cloutier, P. A., Connerney, J. E. P., et al. (2001). Probing Mars' crustal magnetic field and ionosphere with the MGS Electron Reflectometer. *Journal of Geophysical Research: Plan*, *106*(E10), 23419–23427. https://doi.org/10.1029/2000JE001435

Vignes, D., Acuña, M. H., Connerney, J. E. P., Crider, D. H., Rème, H., & Mazelle, C. (2004). Magnetic flux ropes in the Martian atmosphere: Global characteristics. *Space Science Reviews*, *111*(1), 223–231. https://doi.org/10.1023/B:SPAC.0000032716.21619.f2

Wilmot-Smith, A., Priest, E., & Hornig, G. (2005). Magnetic diffusion and the motion of field lines. *Geophysical & Astrophysical Fluid Dynamics*, *99*(2), 177–197. https://doi.org/10.1080/03091920500044808

Withers, P. (2009). A review of observed variability in the dayside ionosphere of Mars. *Advances in Space Research*, *44*(3), 277–307. https://doi.org/10.1016/j.asr.2009.04.027

Withers, P., Vogt, M., Mayyasi, M., Mahaffy, P., Benna, M., Elrod, M., et al. (2015). Comparison of model predictions for the composition of the ionosphere of Mars to MAVEN NGIMS data. *Geophysical Research Letters*, *42*(21), 8966–8976. https://doi.org/10.1002/2015GL065205